Ultrasound in Medicine & Biology 50 (2024) 1573–1584

Contents lists available at ScienceDirect

Ultrasound in Medicine & Biology

journal homepage: www.elsevier.com/locate/ultrasmedbio

Original Contribution

Investigation of Ultrasound Mediated Extravasation of a Model Drug by Perfluorobutane Nanodroplets

Qiang Wu [a], Victor Choi [a], Luca Bau [a], Dario Carugo [b], Nicholas D. Evans [c,d], Eleanor Stride [a,b,*]

[a] Institute of Biomedical Engineering, Department of Engineering Science, University of Oxford, Oxford, UK
[b] Botnar Institute for Musculoskeletal Sciences, Nuffield Department of Orthopaedics, Rheumatology and Musculoskeletal Sciences (NDORMS), University of Oxford, Oxford, UK
[c] Centre for Human Development, Stem Cells and Regenerative Medicine, Bone and Joint Research Group, University of Southampton, Southampton, UK
[d] Bioengineering Sciences Group, Institute for Life Sciences, University of Southampton, Southampton, UK

ARTICLE INFO

Keywords:
Ultrasound
Drug delivery
Cavitation
Nanodroplets
Acoustic droplet vaporization
Phase change agents
Stimuli responsive particles

ABSTRACT

Objective: Perfluorocarbon nanodroplets (NDs) have been widely investigated as both diagnostic and therapeutic agents. There remains, however, a challenge in generating NDs that do not vaporize spontaneously but can be activated at ultrasound pressures that do not produce unwanted bioeffects. In previous work, it has been shown that phospholipid-coated perfluorobutane (PFB) NDs can potentially overcome this challenge. The aim of this study was to investigate whether these NDs can promote drug delivery.
Methods: A combination of high-speed optical imaging and passive cavitation detection was used to study the acoustic properties of the PFB-NDs in a tissue mimicking phantom. PFB-NDs were exposed to ultrasound at frequencies from 0.5 to 1.5 MHz and peak negative pressures from 0.5 to 3.5 MPa. In addition, the penetration depth of two model drugs (Nile Red and 200 nm diameter fluorescent polymer spheres) into the phantom was measured.
Results: PFB NDs were found to be stable in aqueous suspension at both 4°C and 37°C; their size remaining unchanged at 215 ± 11 nm over 24 h. Penetration of both model drugs in the phantom was found to increase with increasing ultrasound peak negative pressure and decreasing frequency and was found to be positively correlated with the energy of acoustic emissions. Extravasation depths >1 mm were observed at 0.5 MHz with pressures <1 MPa.
Conclusion: The results of the study thus suggest that PFB NDs can be used both as drug carriers and as nuclei for cavitation to enhance drug delivery without the need for high intensity ultrasound.

Introduction

Superheated perfluorocarbon (PFC) nanodroplets (NDs) are a type of stimulus-responsive nanoparticle that have garnered significant attention for their potential in ultrasound-based diagnostic imaging and drug delivery [1,2]. Multiple studies have shown that PFC NDs can be vaporized by exposure to ultrasound. The resulting gas microbubbles can be easily imaged and the rapid phase change taking place during vaporization can be used to trigger the delivery of therapeutic agents at a target site, by the release of drug molecules encapsulated within or conjugated to the ND surface, and/or to promote localised vascular permeabilization [3,4]. The oscillation of the resulting gas microbubble can also enhance penetration of the drug into the extravascular tissue. The smaller size and greater stability of PFC NDs compared with pre-formed gas microbubbles allows them to more efficiently perfuse the smallest capillaries in the circulatory system, to circulate for longer, and potentially to extravasate through compromised and/or leaky vessels [5,6].

Despite these advantages and the relatively substantial literature already demonstrating the potential of PFC NDs across multiple applications (Table 1), challenges still remain in formulating NDs that can be vaporized at sufficiently low ultrasound pressures to avoid undesired bio-effects in the surrounding tissue. Perfluoropentane (PFP) and perfluorohexane (PFH) have been widely used to form the core of NDs, but these both require substantial acoustic pressure amplitudes to achieve vaporization. Sheeran et al. [7] proposed a method whereby perfluorobutane (PFB), which is gaseous at 20°C at atmospheric pressure, can be used to produce liquid NDs by a gas microbubble condensation technique. They found that NDs produced in this way require significantly lower acoustic pressures to undergo vaporization and subsequent inertial cavitation than PFH or PFP NDs, and that these pressure levels are not substantially higher than those used in therapeutic applications of microbubbles. Indeed, recent studies have used PFB NDs for drug delivery at specific target regions of the brain for non-invasive neuromodulation and localized anesthesia [8]. Despite brain being a highly

* Corresponding author: Botnar Research Centre, University of Oxford, Windmill Road, Oxford OX3 7LD, UK.
E-mail address: eleanor.stride@eng.ox.ac.uk (E. Stride).

https://doi.org/10.1016/j.ultrasmedbio.2024.06.016
Received 9 February 2024; Revised 14 June 2024; Accepted 29 June 2024

Table 1
US-mediated nanodroplet delivery

Study	Core	Shell	Mean Size (nm)	Model System	Bioactive Agent	US Frequency (MHz)	Pressure/ Intensity
Zhao et al. 2023 [28]	PFH	Fluoro-surfactant	302 ± 12	In vivo – mouse	Paclitaxel / L-arginine	1.0	1.5 W/cm^2
Xiao et al. 2023 [29]	PFH	Polymer	146 ± 11	In vivo – mouse	Mn-protoporphyrin IX	3.0	1.5 W/cm^2
Samani et al. 2023 [30]	PFH	Polymer	26.7 ±1.5	In vivo - mouse	Folic acid-methotrexate	1.0	1.0 W/cm^2
Yamaguchi et al. 2023 [31]	PFH	Lipid	66.8	In vitro	β-galactosidase	5.0	4.6 MPa
Hou et al. 2022 [32]	PFH	Polymer	256 ± 3	In vivo – mouse	Dextran sulphate	1.0	2.5 W/cm^2
Zamani et al. 2022 [33]	PFH	Polymer	162 ± 2	In vitro	Doxorubicin	0.028 / 1.0	0.34 / 2 W/cm^2
Shar et al. 2022 [34]	PFH	Protein	200 ± 50	In vitro	Cathepsin K siRNA	1.0	3 W/cm^2
Wang et al. 2022 [35]	PFH	Lipid	266.2	In vivo – mouse	Hydroxychloroquine	1.0	1.5 W/cm^2
Gao et al. 2021 [36]	PFH	Polymer	133 ± 2	In vivo – mouse	Doxorubicin	12	MI = 0.8
Xie et al. 2023 [37]	PFP	Lipid	199 ± 8	In vivo – mouse	Glucose oxidase	Not mentioned	1.6 W/cm^2
Spatarelu et al. 2023 [38]	PFP	Lipid	332 ± 14	In vivo – mouse	Paclitaxel / Doxorubicin	0.515	5.7 MPa
Huang et al. 2023 [39]	PFP	Lipid	440 ± 25	In vivo – mouse	Fe_3O_4 NPs / Doxorubicin	1.0	3 W/cm^2
Xi et al. 2022 [40]	PFP	Lipid	287 ±8.1	In vivo – mouse	Hematoporphyrin (HMME)	1.0	3 W/cm^2
Yang et al.2022 [41]	PFP	Polymer	216 ± 63	In vivo – mouse	Doxorubicin	Not mentioned	3 W/cm^2
Yang et al. 2020 [42]	PFP	Lipid	337 ± 70	In vivo – mouse	Hematoporphyrin (HMME)	1.0	1.5 W/cm^2
Dong et al. 2020 [43]	PFP	Lipid	271 ± 70	In vivo – mouse	Pre-miRNA plasmid	1.2	6.5 – 8.5 MPa
Zhang et al. 2019 [44]	PFP	Lipid	354 ±156	In vivo – mouse	IR780	0.65	0.8 – 4.0 W/cm^2
Ho et al. 2018 [45]	PFP	Lipid	382 ± 4	In vivo – mouse	Camptothecin	2.0	12 MPa
Lee et al. 2017 [46]	PFP	Polymer	258 ± 11	In vitro	Cell death control siRNA	0.5	1.0 MPa
Wang et al. 2012 [47]	PFP	Lipid	480 ± 44	In vitro	Doxorubicin	3.5	11 MPa
Lee et al. 2015 [18]	PFP	Protein-Polymer	416 ± 25	In vitro	Paclitaxel	1.85	0.265 MPa
Gouveia et al. 2023[13]	PFB	Lipid	210 ± 80	In vivo – mouse	Pentobarbital	1.78	2 ± 0.2 MPa
Lea-Banks and Hynynen 2021 [48]	PFB	Lipid	206 ± 6	In vivo – rat	Nile Red	1.66	0.2 – 3.5 MPa
Lea-Banks et al. 2020 [49]	PFB	Lipid	210 ± 80	In vivo – rat	Pentobarbital	0.58	0.5 – 1 MPa
Wu et al. 2018 [50]	PFB	Lipid	182 ± 3	In vivo – mouse	40 kDa FITC-Dextran	1.5	0.75 – 0.9 MPa
Honari et al. 2021 [51]	OFP	Lipid	652 ±120	In vivo – mouse	Fluorescein Liposomes	7.0	2.0 MPa
Fix et al. 2019 [52]	OFP	Lipid	170 ± 20	In vitro	70 kDa FITC-Dextran	1.0	0.3 – 0.6 MPa
Wu et al. 2018 [50]	OFP	Lipid	171 ± 3	In vivo – mouse	40 kDa FITC-Dextran	1.5	0.15 – 0.45 MPa
Fix et al. 2017 [53]	OFP	Lipid	NR	In vitro	Bleomycin	1.0	0.4 MPa
Choi et al. 2022 [54]	PFD	Polymer	219.6	In vitro	Nile Red	1.0	3.0 W/cm^2

PFH, Perfluorohexane; PFP, Perfluoropentane; PFB, Perfluorobutane; OFP, Octafluoropropane; PFD, Perfluorodecalin.

mechanosensitive organ, no signs of toxicity in histological analyses nor oedema and red blood cell extravasation could be observed following ND-based treatment. Previous work, however, has suggested that NDs may not be as effective at promoting the extravasation of drug molecules and/or therapeutic particles as other types of cavitation agent [9]. This is of particular importance for applications involving poorly vascularized tissue such as some types of solid tumour and bone fracture sites. The aim of this study was to investigate whether PFB NDs could be used to promote the extravasation of model therapeutics in a tissue mimicking phantom and to evaluate their loading capacity, release characteristics and cytotoxicity *in vitro*.

Materials and methods

Materials

The following compounds were purchased from Sigma-Aldrich Inc.: 1,2-distearoyl-sn-glycero-3-phosphocholine (DSPC), 1,2-distearoyl-sn-glycero-3-phosphoethanolamine-N-[methoxy(polyethylene glycol)-2000] (DSPE-PEG2000), phosphate-buffered saline (PBS), Nile red, 3,3′-Dioctadecyloxacarbocyanine perchlorate (DiO), ethanol, and dimethylsulfoxide (DMSO). These compounds were used without further purification. 200 nm amine-modified yellow-green fluorescent spheres (ThermoFisher, Waltham, MA, USA), UltraPure Agarose-1000 (Invitrogen, Paisley, UK), CellTiter 96 AQueous One Solution Cell Proliferation Assay (MTS, Premega Corporation, USA) and perfluorobutane (PFB, FluoroMed, L.P. USA) were also used without further purification. Ultrapure deionized water was obtained from a Millipore Milli-Q plus system (Millipore S.A.S., France).

Synthesis of NDs

Firstly, 20 mg of 90 mol% DSPC and 10 mol% DSPE-PEG2000 were dissolved in chloroform (total lipid concentration: 25 mg/mL), followed by evaporation to form a thin dry film. Then the resulting lipid films were hydrated in 4 mL of PBS/propylene glycol/glycerol (16:3:1 volume ratio) solution. To generate fluorescently labeled NDs, DiO was added to the chloroform solution to achieve a final molar concentration of 10 μM. For the model drug release experiments, Nile red was added to the chloroform solution to achieve a final molar concentration of 0.4 mM. To generate the NDs, PFB gas was condensed by injecting it into a scintillation vial cooled at −12 °C in an ethanol/ice bath. 100 μL of the resulting PFB liquid was added to the lipid suspension. The mixture was sonicated using a probe sonicator (tip diameter 3 mm, Q125, QSonica, LLC., USA) in an ethanol ice bath maintained between -7 °C and -12 °C at 50% amplitude for 3 minutes (125 W, 20 kHz, pulsed mode: 2 s on and 4 s off). To remove excess free lipids, the resulting ND emulsion was centrifuged at 10,000 rpm (11,292 g) for 6 min and resuspended in fresh PBS. The centrifugation and washing steps were repeated three times. The prepared NDs were stored at 4 °C for later use.

Characterization of NDs

The hydrodynamic diameter of the PFB NDs was first measured using dynamic light scattering (DLS) with a Zetasizer Nano ZS instrument (Malvern Panalytical, Malvern, UK) at a temperature of 20°C. Three independent samples for each batch were analyzed. The morphology and size of the NDs were further characterized by cryogenic transmission electron microscopy (Cryo-TEM) using a Talos Arctica TEM machine (Thermo Fisher Scientific, Hillsboro, Oregon; USA). The ND sample was transferred to lacey carbon grids, which were frozen using a Thermo Fisher Vitrobot Mark IV prior to imaging. The size of the NDs in the TEM images was measured by ImageJ software (National Institutes of Health, Bethesda, MD, USA). The concentration and size of PFB NDs dispersed in PBS were also quantified using nanoparticle tracking analysis (NTA) on a NanoSight LM-20 instrument (NanoSight, Wiltshire, UK) with NTA software (Version 3.0, Build 0066, Malvern Instruments, Malvern UK).

Stability of NDs

The stability of PFB NDs was measured in PBS at storage temperature (4°C) and physiological temperature (37°C) by monitoring changes in ND size and concentration at each time point using DLS and NTA, respectively. PBS was used as the suspending medium for consistency with previous studies.

Acoustic response of NDs

The acoustic response of PFB NDs was evaluated using a modified version of the experimental set up described by Wu et al. [10] and shown in Figure 1. Briefly, NDs were drawn through a 1.2 mm inner diameter and 0.2 mm wall thickness polyethylene tube (Advanced Polymers, Salem NH, USA) at a constant volumetric flow rate of 0.3 mL/min (corresponding to a 4.42 mm/s mean velocity) using a low-pulsatility peristaltic pump (Minipulse Evolution, Gilson, Middleton, WI, USA) at a concentration of 10^9 particles/mL in degassed PBS. The NDs were acoustically stimulated using a single-element spherically focused ultrasound (FUS) transducer (0.5 MHz and 1.5 MHz center frequency, H107, Sonic Concepts, Bothell, WA, USA). A second single-element spherically focused FUS transducer with a center frequency of 1.0 MHz (H102 Sonic Concepts, Bothell, WA, USA) was also used to stimulate the NDs in this setup. Both transducers' aperture and geometric focus were 64 and 63.2 mm, respectively. A third ultrasound transducer, characterized by central frequency of 7.5 MHz, element diameter of 12.5 mm, and focal length of 75 mm (V320 Panametrics, Olympus, Waltham, MA, USA), was employed in the capacity of a passive cavitation detector (PCD). This transducer was strategically positioned by inserting it through a circular aperture in the FUS transducer, ensuring precise alignment between the foci of both transducers. The transducer employed for ND stimulation was driven by a programmable arbitrary waveform generator (33220 A, Agilent, Santa Clara, CA, USA) and the US field was focused on the polyethylene tube. The signal was amplified with a 300 W radiofrequency power amplifier (A-300, ENI, USA) and sent to the FUS transducer *via* a 50 Ω matching network. The tube and transducer were placed in a degassed and deionized water tank. All experiments were performed at 37°C. The PCD signal was filtered using a 5 MHz high-pass filter (F5081-5 P00-B, Allen Avionics, Inc., River Grove, IL, US; 20-dB bandwidth of 3.125 MHz) to eliminate strong reflections from the tube at the fundamental FUS frequency and lower harmonics resulting from non-linear propagation. The filtered signal was amplified five times using a low-noise amplifier (SR445 A, Stanford Research Systems, Sunnyvale, CA, USA) and recorded using a 14-bit PCI oscilloscope (PCI-5122, National Instruments, Austin, TX, USA) at a rate of 100 MHz. The frequency spectra of the emissions captured by the PCD were analysed to determine the PFB NDs' response to ultrasound. MATLAB (Mathworks, Natick MA, USA) was utilized for all data analysis. A high-speed camera (HPV-X2, Shimadzu, Tokyo, Japan) coupled with an objective lens with a numerical aperture of 0.45 and working distance of 8.2−6.9 mm (S Plan Fluor, Nikon Instruments Europe BV, Amsterdam, Netherlands) was focused on the tube's midplane. The high-speed camera was triggered by the waveform generator output after a delay of 40 μs to allow sufficient time for ultrasound pulse propagation to the focal region. A high-intensity light source (SOLIS-445 C, Solis High-Power LEDs, Thorlabs LTD. Ely, UK) provided illumination in the setup. The camera recorded 256 frames at a rate of 5 million frames per second (Mfps), with an exposure time of 200 ns per frame, providing a temporal resolution of 0.2 μs. Digital images were obtained at a resolution of 0.34 μm/pixel, based on calibration with a haemocytometer reference standard (Bright-Line, Hausser Scientific, Horsham, PA, USA). The images had a size of 400 × 250 pixels.

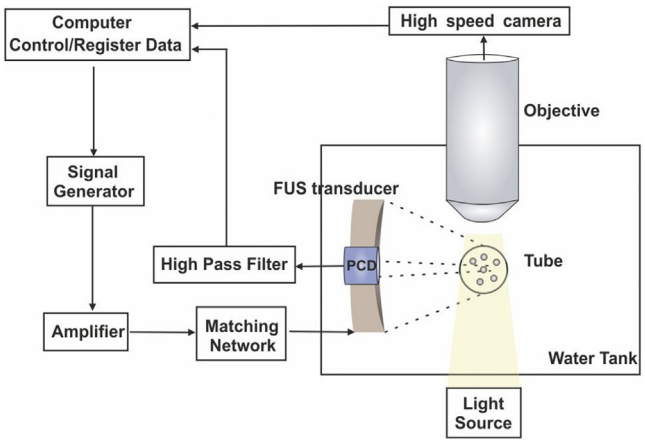

Figure 1. Schematic diagram of the experimental setup employed for simultaneous optical and acoustic measurements, containing the focused ultrasound transducer (FUS), PCD transducer, high speed camera.

Cavitation analysis

For the purposes of inertial cavitation (IC) measurements, a PCD recording with a duration of 5000 μs was synchronized with the initiation of every fifth pulse generated by the FUS transducer. The frequency spectra of acoustic emissions, captured by the PCD, were systematically computed through the implementation of the Fast Fourier Transform (FFT) method. Separation of harmonic components and broadband noise was achieved through the application of a comb filter with a width of 300 kHz. This computational analysis was executed using MATLAB (R12 The Mathworks, Natick, MA, USA). Inertial cavitation events were identified when the mean-squared amplitude of the broadband signal surpassed that of the background noise by a minimum factor of 20 (i.e., e^3). The probability of inertial cavitation (PIC) was calculated as the ratio of instances where IC was detected to the total number of pulses generated. IC thresholds were defined as the peak negative driving pressures producing a PIC > 80%. This threshold was selected for its ability to provide an acceptable degree of repeatability across experiments based on previous work [11].

Release of Nile red as a model drug from PFB NDs upon ultrasound exposure

To investigate drug release from PFB NDs, Nile red was used as a model drug. Nile red-loaded PFB NDs were produced as described above. The amount of Nile red encapsulated in the NDs was determined using a fluorescence plate reader (FLUOstar Omega, BMG Labtech, UK). 900 µL of a mixture of ethanol and DMSO (1:1) was added to 100 µL of ND suspensions diluted in PBS in a 1:20 ratio samples. The quantity of Nile red was then determined by comparing the fluorescence measurements with a previously constructed standard curve. This curve was generated by measuring the fluorescence intensity of Nile red in a solution comprising PBS, ethanol and DMSO at a ratio of 2:9:9, across various concentrations of Nile red. Encapsulation efficiency (EE, %) was calculated by the following eqn (1):

$$EE\ (\%) = \frac{The\ amount\ of\ Nile\ Red\ encapsulated\ in\ PFB\ NDs}{The\ amount\ of\ Nile\ Red\ added\ before\ sonication} * 100 \qquad (1)$$

The initial Nile red loaded NDs were diluted at a ratio of 1:20 for the release experiment, to achieve a concentration of released Nile red that was suitable for measurement using the standard curve. Unloaded NDs and Nile red loaded NDs were exposed to ultrasound for 15, 30, 60, 90, 120, 180, or 300 s respectively, using an *in vitro* "SAT2" system previously described by Gray et al. [12] In this system, a 1.0 MHz centre frequency ultrasound source (Imasonic 8233 A101, 40 mm diameter, 120 mm radius of curvature) is located at the base of a cylindrical water tank and fed by a radio frequency amplifier (1020L, E&I Ltd., 200 W power amplifier) that is driven by a waveform generator (33250,

Agilent). The SAT2 cell exposure compartment is established through the aseptic assembly of a deformable polydimethylsiloxane (PDMS) lid onto a designated culture dish (35 mm in diameter, Ibidi, Germany), following a protocol described previously [12]. Notably, the PDMS lid is designed with a pair of precisely machined 1.2 mm diameter apertures, specifically positioned to enable priming of the compartment through an 18-G blunt needle connected to a syringe. NDs were injected into a culture dish, which was submerged in the water tank at the transducer's focus and exposed to ultrasound. The peak rarefactional pressure, number of cycles and duty cycle were set to 1.5 MPa, 5000 cycles and 10%, respectively. All experiments were performed at 37°C. After ultrasound exposure, 100 μL samples were extracted from the dish, transferred into 2 mL Eppendorf tubes and then centrifuged to remove the NDs. Subsequently, 900 μL of a mixture of ethanol and DMSO (1:1) was added to the supernatant and gently shaken. The fluorescence intensity of the sample was subsequently measured at an emission wavelength of 630 nm, with an excitation wavelength of 530 nm, using the plate reader. The amount of Nile red released was then calculated *via* comparison with the previously determined standard curve.

In vitro evaluation of drug extravasation

The experimental setup from Figure 1, was modified to test drug penetration *in vitro* as shown in Figure 2. The polyethylene tube was replaced by a degassed biocompatible hydrogel composed of 1.25% (w/v) low melting point UltraPure™ Agarose-1000 (Invitrogen, Carlsbad, CA, USA). This hydrogel construct was employed as a tissue mimicking phantom for consistency with previous studies of drug extravasation [9]. The pore diameter of the gel vessel phantom is approximately 500 nm, a dimension comparable to the endothelial gap found in tumor tissue [13]. The phantom was fabricated by a controlled heating and cooling process: a 1.25% (w/v) agarose solution was subjected to microwave treatment in PBS, cooled to 50°C and then poured into a rectangular container with three cylindrical metallic mandrels of diameter 1 mm traversing it. The phantom was allowed to solidify at 4°C overnight. Following gel solidification, the metallic mandrels were removed, resulting in the formation of three flow-through channels approximately 1 mm in diameter and 50 mm in length. This configuration facilitated the testing of multiple experimental conditions within the same gel manifold and thereby reduced experimental variability. The overall thickness of the phantom amounted to 12 mm.

Three FUS transducers having different fundamental frequencies (0.5, 1.0, and 1.5 MHz) were used to excite the PFB NDs, while the same 7.5 MHz spherically focused PCD transducer (V320 Panametrics, Olympus, Waltham, USA) was used to record any acoustic emissions. The same peristaltic pump was used to draw NDs in de-gassed PBS through each channel, at a constant rate of 0.3 mL/min. The acquired PCD signal was processed and recorded as described above. An ultrasound imaging probe (L12-5 linear array, operated at 7 MHz using an iU22 imaging system, Philips, Bothell, WA, USA) was also used to simultaneously record B-mode images from the channel with the aim of detecting ND vaporization. Again, all experiments were performed at 37°C.

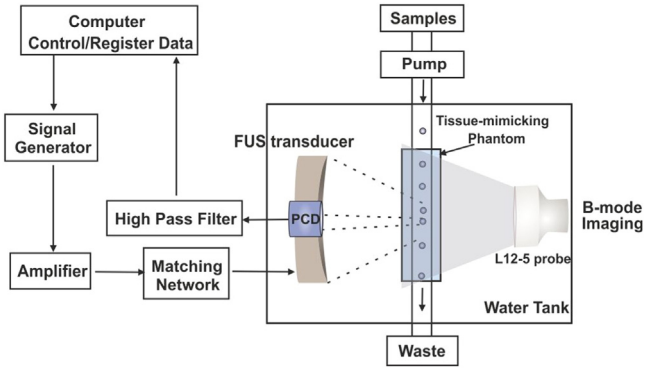

Figure 2. Schematic diagram of the experimental setup for in vitro evaluation of drug extravasation, containing the focused ultrasound transducer (FUS), PCD transducer, tissue-mimicking phantom and diagnostic ultrasound imaging device.

To simulate delivery of large macromolecular therapeutics such as gold nanoparticles or oncolytic viruses, 200 nm amine-modified yellow-green fluorescent spheres (Ex/Em: 505nm/515nm, ThermoFisher, Waltham, MA, USA) were used as model drug and were added to the PFB ND suspension prior to each experiment. 1 μL of a 20 mg/mL suspension of the model drug particles was added into 1 mL of the ND suspension (10^9 ND/mL), before injection into the phantom. Each suspension was checked for possible inter-particle aggregation prior to each experiment, using DLS to assess whether there was a significant increase in detected particle size, but none was observed. For comparison, nanospheres (NPs) were added into degassed water to repeat the experiments with the same parameters. In addition, Nile red loaded NDs were used to investigate extravasation of small molecule drugs. Following ultrasound exposure, the flow channels were flushed with deionized water and the hydrogel phantom was then sectioned through and along each channel using a scalpel. The obtained hydrogel slices were placed onto a glass microscope slide (1 mm thick) for examination using an inverted fluorescence microscope (Eclipse Ti, Nikon Inc, USA). The farthest vertical distance between detected fluorescent spheres and the upper edge of the channel in the images was defined as extravasation depth.

Cell culture

Immortalized human alveolar adenocarcinoma cells (A549 cells) were used as a model cell line to assess cytotoxicity and uptake of NDs. The cells were cultured in Dulbecco's modified Eagle's medium (DMEM) supplemented with 10% (v/v) fetal bovine serum and maintained in an incubator with a humidified atmosphere containing 5% CO_2 at 37°C. Cells in logarithmic growth phase were used for these experiments. Cell concentrations were measured using a Countess® Automated Cell Counter (Invitrogen, UK). All cell culture reagents were purchased from ThermoFisher Scientific (UK).

Cytotoxicity of PFB NDs

The cytotoxicity of PFB NDs was evaluated using an MTS assay (Life Technologies Ltd., UK) according to the manufacturer's protocol. A549 cells were seeded in a 96-well plate at a density of 5×10^3 cells per well in medium (100 μL) for 24 hours. The medium was then replaced with fresh medium (100 μL) containing PFB NDs at different particle concentrations (10^6~10^{11} particles/mL). After a further 24 h of incubation, the cells were rinsed with PBS and treated with MTS reagent (10% in medium) for 2 h. The absorbance at 490 nm of the medium was measured using a plate reader (FLUOstar Omega, BMG Labtech, Germany).

Cellular uptake of NDs

The cellular uptake of DiO-loaded PFB NDs by A549 cells was investigated by confocal microscopy. The localization of PFB NDs was visualized and detected by confocal laser scanning microscopy (Zeiss LSM 780, Carl Zeiss AG, Germany), leveraging the intense fluorescence property of the DiO dye when incorporated within PFB NDs. A549 cells were seeded in a 96-well plate at a density of 5×10^3 cells per well in medium (100 μL) for 24 h. The medium was then replaced with fresh medium (100 μL) containing PFB NDs at a concentration of 10^9 particles/mL. After 2 h of incubation with NDs, the cells were rinsed with PBS and were finally imaged with the LSM780 confocal microscope using the Zen software (Carl Zeiss). The imaging utilized a Plan-Apochromat 63×/NA 1.4 oil objective and a 488 nm laser for excitation. Images at a

resolution of 1024 × 1024 pixels were acquired and processed using Zen software.

Statistical analysis

All statistical analysis was performed in R (version 4.3.1). Linear mixed models (for mean diameter stability) were estimated with the *lme4* package, while nonlinear mixed models (for concentration stability) were estimated with the *nlme* package. In both cases, random effects on the intercepts were used to account for within-sample correlation. Confidence intervals (CI) on coefficients and confidence bands on predictions were obtained by parametric bootstrapping (10,000 resamples). PIC was fitted to Weibull cumulative distribution functions except for NDs at 0.5 MHz, which was fitted to a bi-Weibull cumulative distribution function. Pressure thresholds and the corresponding confidence intervals were obtained by parametric bootstrapping (10,000 resamples). Extravasation depth was modelled as a log-logistic function of pressure, fixing the lower and upper bounds to 0 and 5.5 mm (the maximum depth of the phantom), respectively. A 5-parameter log-logistic function was used for NDs + Nile red and NDs + Nanospheres at 0.5 MHz, and a 4-parameter log-logistic function was used for the rest. Pressure thresholds and the corresponding confidence intervals were obtained with the delta method. Simultaneous confidence bands on both PIC and extravasation depth were estimated from standard errors obtained with the delta method and a critical value calculated with the sup-t method. Cell viability was fitted to an exponential model and the concentration required to cause a 15% decrease in cell viability (benchmark dose, BMD) and its corresponding confidence interval were obtained with the delta method. Differences between estimates with non-overlapping 95% confidence intervals or non-overlapping 95% simultaneous confidence bands were deemed statistically significant (at an alpha level of 0.05).

Results and discussion

Characterization of PFB NDs

It has been shown that particle size can affect *in vivo* pharmacokinetics, as it impacts on circulation time, biodistribution, and cellular uptake, thereby influencing the feasibility and efficacy of both imaging and therapy [14]. Furthermore, PFC ND size has been shown to influence the pressure required for acoustic vaporization [10]. Thus, accurate measurement of ND size is important. In this study, the size of PFB NDs was measured using DLS, NTA and Cryo-TEM. Figure 3a shows a schematic of a Nile red-loaded PFB ND. Figure 3b shows the size distribution of PFB NDs measured by DLS, which indicated a mean diameter of 215 ± 11 nm (polydispersity index (PDI) = 0.137). The NTA measurements returned a mean diameter of 176 ± 19 nm, as shown in Figure 3c. The mean diameter of PFB NDs measured from the cryo-TEM images was 164 ± 40 nm (Figure 3e). The difference in the measured size distributions may be attributed to the different measurement principles of these three techniques. In DLS, the sample is illuminated by a laser beam and the fluctuations of the scattered light produced by particles moving under Brownian motion are detected at a known scattering angle by a fast photon detector. The size distribution of the particles is then calculated using the Stokes-Einstein relationship. The scattering intensity fluctuations recorded in DLS are sensitive to skewing by the presence of large particles. Thus, the mean size can be overestimated if the particle size distribution is broad and/or multimodal. NTA uses a similar principle but measurements are less susceptible to skewing by large particles as light scattering from particles is measured under flow [15]. Both DLS and NTA measure the hydrodynamic diameter of NDs, which is inevitably larger than the true diameter. In contrast, cryo-TEM directly captures both the dimensions and morphology of individual particles. Cryo-TEM images of NDs show a clear distinction between the perfluorocarbon core, lipid shell, and surrounding medium, as shown in Figure 3d.

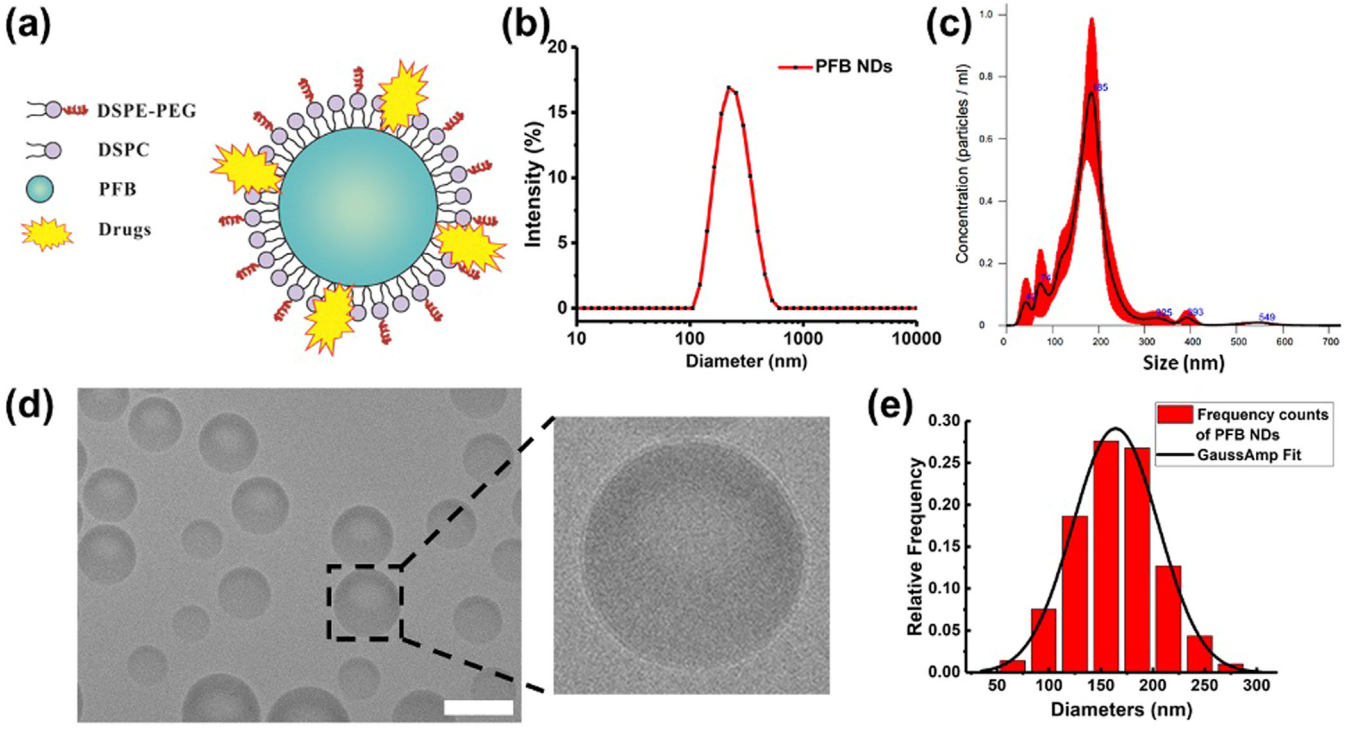

Figure 3. Characterization of PFB NDs. (a) The schematic diagram of a drug loaded PFB ND; size distribution of PFB NDs measured by DLS (b) and NTA (c); (d) cryo-TEM image of PFB NDs, the scale bar is 200 nm; and (e) size distribution of PFB NDs measured from Cryo-TEM images.

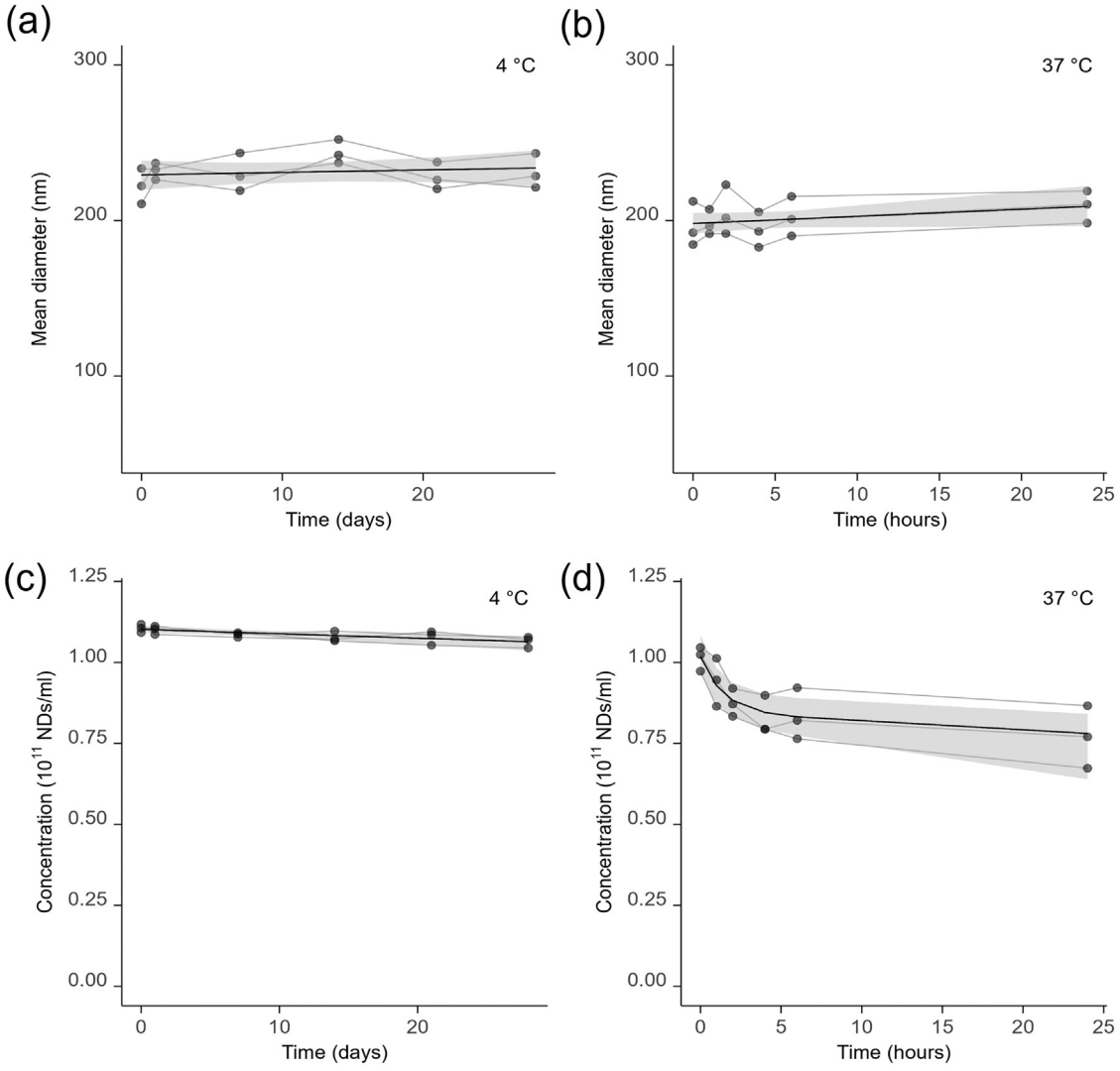

Figure 4. Stability of PFB NDs: the size (a) and concentration (b) change over time at 4°C; the size (c) and concentration (d) change over time at 37°C. The black solid lines are fitted concentrations, the shaded areas are 95% confidence bands.

However, a much smaller number of particles can be practically imaged by cryo-TEM.

Stability of PFB NDs

The stability of the NDs was assessed by measuring their mean diameter over a period of 24 h at 37°C and one month at 4°C in PBS using DLS, as shown in Figure 4a and 4b. The results show that the size remained substantially unchanged for the duration of the investigation at 4°C (0.2 nm/day, 95% CI -0.4−0.8, $p > 0.05$) and at 37°C (0.5 nm/h, 95% CI -0.2 to 1.1, $p > 0.05$).

The concentration of NDs was also measured using NTA. ND emulsions stored at 4°C for one month showed a negligible concentration loss, decreasing by only 3.7% over the storage period, as shown in Figure 4c. The concentration loss was fitted with a nonlinear mixed model as an exponential decay with a half-life of 18 mo (95% CI 10 −36). At 37°C (Figure 4d) the concentration loss was 17.4% ± 7.2% after 6 h, with 75.9% ± 9.1% of NDs still detectable after 24 h. At this temperature, the decay is biphasic, with half-lives of 1 h (95% CI 0.5−1.7) and 8.6 d (95% CI 2.3−44). The stability of these nanodroplets is influenced by multiple factors including environmental temperature, droplet diameter, and the composition of the droplet shell. The lower stability of perfluorobutane nanodroplets at 37°C is due to the temperature dependence of the bubble nucleation rate in superheated liquids. The biphasic decay observed at this temperature is likely due to the size dependence of vaporization rates, with a population of smaller droplets remaining stable, and a population of larger droplets more likely to undergo vaporization due to their larger volume (the nucleation rate within a single droplet being proportional to its volume) and, if the interfacial tension is not negligible, lower liquid pressure. Consequently, this effect explains the observed reduction in the concentration of PFB NDs at 37°C compared to 4°C, reflecting the increased rate of vaporization at the higher temperature.

Acoustic properties of NDs

Acoustic emissions and high-speed videos were captured simultaneously to determine whether the appearance of visible gas bubbles coincided with a change in the acoustic radiation, and hence to evaluate the utility of the latter as a means of detecting ND vaporization. Figure 5 shows representative time traces (first column), their corresponding frequency content (second column), and optical images (third column) at different peak negative driving pressures. The ultrasound frequency, pulse length and pulse repetition frequency (PRF) were 0.5 MHz, 1000 cycles and 10 Hz, respectively. The experimental temperature was set to 37°C and the concentration of PFB NDs was 10^9 particles/mL. The

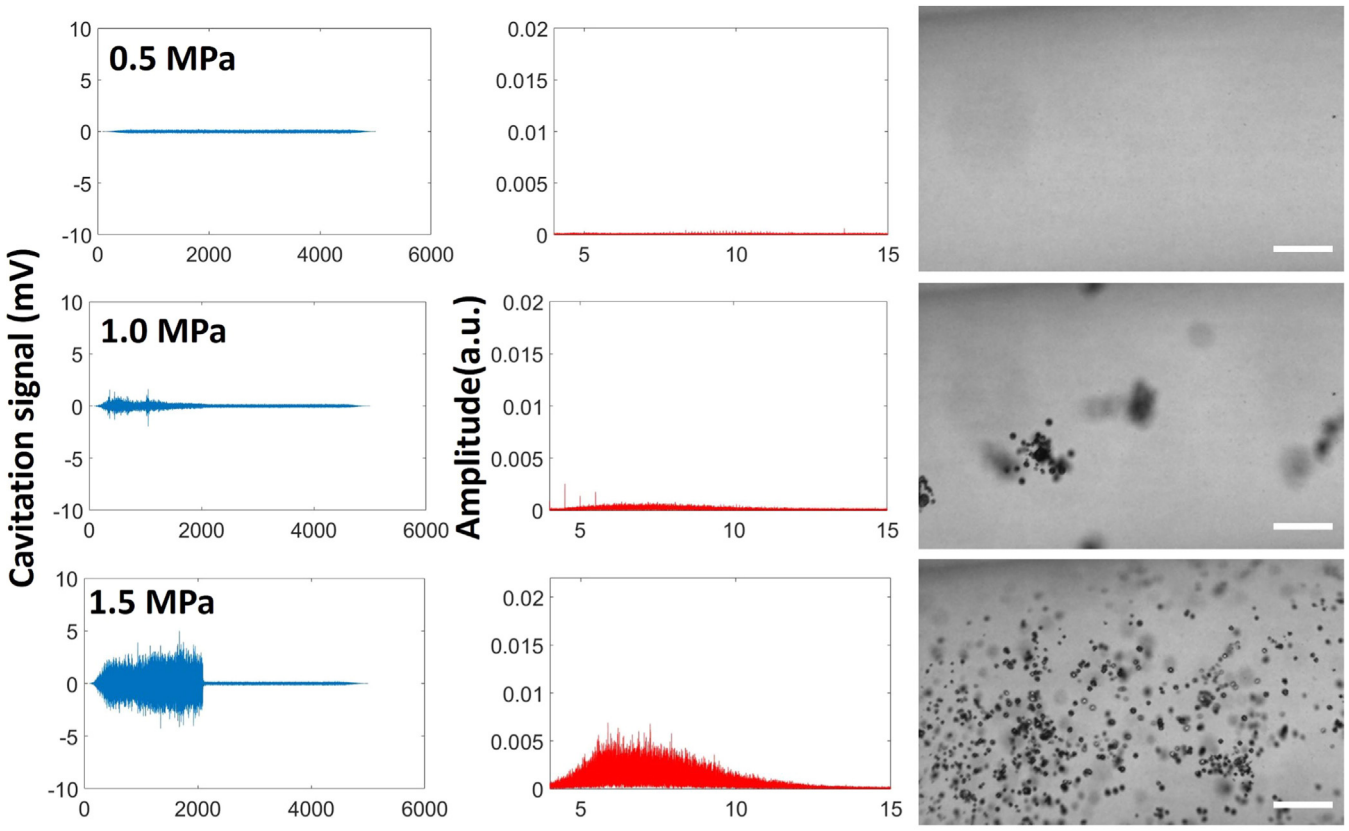

Figure 5. Representative acoustic emissions (first column), their corresponding frequency content (second column) and optical images (third column) from the high-speed videos for NDs exposed to different peak negative pressures. The frequency, pulse length and pulse repetition frequency (PRF) were 0.5 MHz, 1000 cycles and 10 Hz respectively. Scale bar = 20 μm.

amplitude of the acoustic emissions and their broadband noise content similarly increased with increasing pressure. Only a small number of bubbles appeared in the images when the driving peak negative pressure was lower than 1 MPa; but much larger numbers formed at pressures of 1.5 MPa and greater (representative video files are provided in the supplementary materials). The dynamics of bubbles generated from ND vaporization has been detailed in our previous research [10]. Briefly summarized, at the outset of several initial cycles at 1.5 MPa, NDs begin to vaporize and expand during the rarefactional half-cycle, consequently forming a bubble that achieves its maximum size. During the compressional half-cycle, the bubble visibly compresses and ultimately vanishes from detection at the peak of compression. Due to the optical resolution limit (~400 nm), it remains uncertain whether recondensation occurs at these pressures. In comparison, the condensation pressure for PFB microbubbles is around 500 kPa [16], suggesting that recondensation might take place at 1.5 MPa during the compressional half-cycle. Subsequently, the bubble undergoes volumetric oscillations, maintaining a roughly spherical shape across several cycles, yet the bubble's size gradually increases. After several cycles, several bubbles appear in a cluster and these are highly non-spherical, either because of fragmentation and coalescence of the original bubbles or nucleation of additional droplets, and these bubbles expand and contract.

Previous studies have correlated "inertial" cavitation, as indicated by the detection of broadband acoustic emissions, with the extravasation of both molecular and nanoparticulate therapeutics into tissue [9]. Accordingly, the probability of inertial cavitation (PIC) was calculated as the fraction of total pulses for which IC was detected. Figure 6 shows the measured PIC of water and NDs as a function of peak negative pressure at 0.5 MHz (Fig. 6a), 1 MHz (Fig. 6b), and 1.5 MHz (Fig. 6c).

In this study, very low cavitation was observed in degassed water with any method, over the range of ultrasound frequencies and pressures tested, with PIC never exceeding 20%. The dependence of PIC on pressure was fitted to Weibull cumulative distribution functions and the pressure required to achieve 5% PIC was found to be 1.07 MPa (95% CI 0.94-1.22) at 0.5 MHz, 1.76 MPa (95% CI 1.71–1.80) at 1 MHz and 2.82 MPa (95% CI 2.71–2.96) at 1.5 MHz. In contrast, much lower pressures were required to achieve the same PIC with NDs: 0.35 MPa (95% CI 0.23–0.46) at 0.5 MHz, 0.75 MPa (95% CI 0.70–0.80) at 1 MHz and 1.16 MPa (95% CI 1.11–1.22) at 1.5 MHz. Substantial levels of broadband emissions (PIC > 80%) were only observed with NDs, above 1.22 MPa (95% CI 1.20–1.25) at 0.5 MHz, 1.75 MPa (95% CI 1.72–1.79) at 1 MHz and 2.21 MPa (95% CI 2.17–2.25) at 1.5 MHz. As expected, higher pressure was required at higher frequency.

In vitro release of Nile red from PFB NDs upon ultrasound exposure

Figure 7a illustrates the standard curve depicting the fluorescence intensity of Nile red at various concentrations. The encapsulation efficiency of Nile red in PFB NDs was determined to be 89.2% ± 3.5 %. The release of Nile red was quantified by measuring fluorescence intensity both with and without ultrasound exposure. The initial concentration of Nile red in the suspension used for release experiments was 18 μM. In the absence of ultrasound, there was no statistically significant difference in fluorescence intensity between the loaded and unloaded ND suspensions, as shown in Figure 7b. After 1 min of ultrasound exposure (1.5 MPa, 5000 cycles and 10% duty cycle), 30.8% ± 4.4% of the Nile red was released from the NDs compared to initial Nile red encapsulated in PFB NDs, with 78.4% ± 5.3% and 93.4% ± 5.2% released within 2 mins and 5 mins, respectively. Around 80% of the Nile red was released within the initial 120 s of ultrasound exposure, after which drug release plateaued. This rapid release of the majority of the encapsulated drug within a brief time frame is termed "dumping", a phenomenon discussed

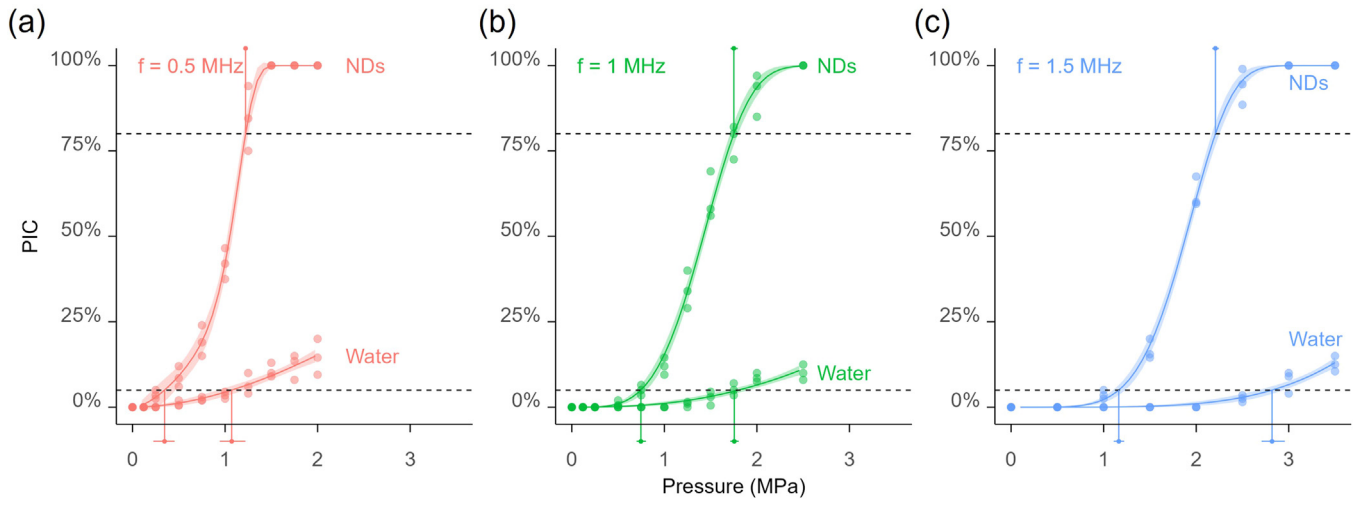

Figure 6. Probability of inertial cavitation (PIC) as a function of peak negative acoustic pressure in perfluorobutane ND (PFB ND) suspensions and water. The frequency, pulse length and pulse repetition frequency (PRF) were 0.5 MHz (a), 1 MHz (b) and 1.5 MHz (c), 1000 cycles and 10 Hz, respectively. The solid lines are fitted concentrations, the shaded areas are simultaneous 95% confidence bands. Pressure thresholds are shown above (for 80% PIC) or below (for 5% PIC) the plots as points with horizontal error bars corresponding to their 95% confidence intervals.

in previous work by Avi Schroeder et al. [17]. Several factors likely contribute to this observed release profile:

1. PFB NDs were transformed into microbubbles upon ultrasound exposure, which induces cavitation. This process generated substantial mechanical forces that can compromise the integrity of drug delivery vehicles, facilitating a swift release of the encapsulated drug. Over prolonged exposure to ultrasound, the intensity of cavitation diminished, which consequently slowed the rate of drug release.
2. Nile red that is adsorbed or weakly bound to the surface of the carrier tends to be released more rapidly due to its immediate availability and direct exposure to the ultrasound. After the release of the surface-associated Nile red, the remaining drug, which is either more centrally located or more tightly bound within the matrix of the nanodroplets, is released at a slower pace owing to reduced accessibility.
3. At the onset of treatment, Nile red tends to diffuse more rapidly out of the matrix, driven by the high concentration gradient between the drug in the matrix and the external medium. As this gradient diminishes, the rate of diffusion and hence drug release decreases.

The results suggest that the release of Nile red from Nile red-loaded PFB NDs is contingent upon ultrasound exposure. Moreover, the release profile demonstrates a significant correlation with the droplet vaporization rate, aligning with previous studies conducted within our research group [18].

In vitro evaluation of drug extravasation

To assess the potential of PFB NDs to enhance drug extravasation, they were first co-administered with 200 nm yellow-green fluorescent nanospheres to simulate a nanoparticulate therapeutic agent. Second, Nile red loaded NDs were used to simulate NDs carrying a small-molecule hydrophobic drug. In both cases, the NDs were perfused through a tissue flow phantom and exposed to 1 MHz, 10 Hz, 5% duty cycle ultrasound at varying pressure levels for 1 minute. Figure 8 shows examples of side- and top-view fluorescence images of sections excised from the phantom around locations exposed to ultrasound. Consistent with the PIC results above (Figure 10), no detectable extravasation was observed with a peak negative driving pressure of 1 MPa. The IC threshold (PIC>80%) was found to be 2 MPa at 1 MHz and Figure 8a shows that

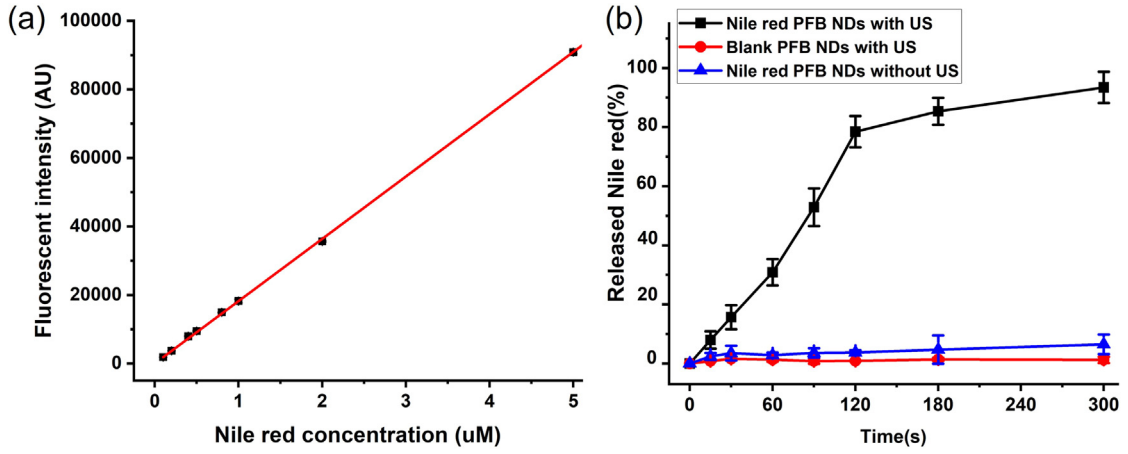

Figure 7. (a) Standard curve between fluorescence intensity and Nile red concentration. (b) Release profiles of Nile red from Nile red loaded PFB NDs and blank PFB NDs with varying ultrasound exposure times, and from Nile red loaded PFB NDs without ultrasound exposure. The peak rarefactional pressure, number of cycles, and duty cycle were set to 1.5 MPa, 5000 cycles and 10%, respectively.

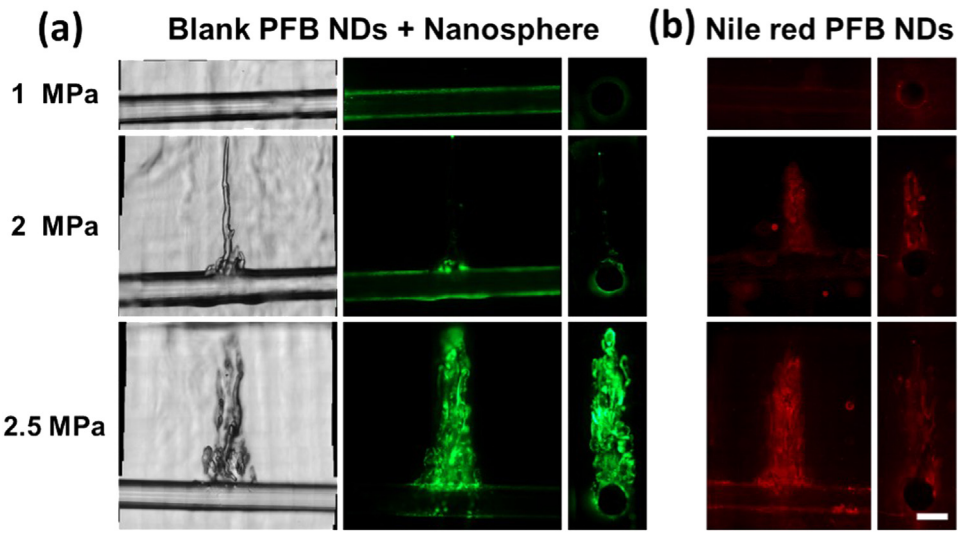

Figure 8. (a) Representative microscopy images of nanosphere extravasation in the agarose phantom model under different ultrasound pressures at 1 MHz at the same duty cycle (5%), showing bright field (left), and green fluorescence images of the top (centre) and side (right) view of the channel. (b) Representative microscopy images of Nile red extravasation in the agarose phantom model under different ultrasound pressures at 1 MHz at the same duty cycle (5%), showing red fluorescence images of the top (left) and side (right) view of the channel. The scale bars represent 1 mm.

nanoparticle extravasation started to occur at a driving pressure of 2 MPa and became significant at 2.5 MPa. In the absence of NDs, no detectable extravasation was observed under the same ultrasound exposure conditions. Similar results were obtained with the Nile red loaded NDs. As shown in Figure 8b, Nile red extravasation was detected for driving pressures of 2 MPa and 2.5 MPa.

The effect of ultrasound frequency on ND extravasation was also examined by repeating the experiment at 0.5 and 1.5 MHz. The 80% PIC threshold was found to be 1.25 MPa at 0.5 MHz, 5% duty cycle, and 10 Hz and significant extravasation was detected at 1 MPa at this frequency (Figure 9a). The IC threshold for PFB NDs at 1.5 MHz was found to be 2.5 MPa and correspondingly no extravasation was observed at 1 MPa at this frequency (Figure 9b), although measurable extravasation did occur once the pressure was increased to 2 MPa. The extravasation depth increased with increasing driving pressure at each ultrasound frequency, as illustrated in Figure 9c, consistent with the relationship between PIC and pressure. The lowest pressure required for extravasation was found to be 0.5 MPa at 0.5 MHz. At 1.5 MPa and a frequency of 1.5 MHz, no extravasation was observed. However, at the same pressure of 1 MHz, the extravasation depth was 1.2 ± 0.3 mm, and at 0.5 MHz, it was 5.2 ± 0.2 mm. Upon increasing the pressure to 2.5 MPa, the extravasation depths at 0.5 MHz, 1 MHz, and 1.5 MHz were 5.5 mm (i.e. the edge of the phantom), 4.9 ± 0.6 mm, and 1.5 ± 0.3 mm, respectively. In contrast, when nanospheres were subjected to ultrasound in the absence of nanodroplets at 2.5 MPa, the extravasation depths achieved at frequencies of 0.5 MHz, 1 MHz, and 1.5 MHz were 0.5 ± 0.2 mm, 0.3 ± 0.1 mm, and 0.2 ± 0.1 mm, respectively. Extravasation depth was fitted to an empirical model using a log-logistic function of pressure. The pressure required to achieve an extravasation depth of 0.3 mm was 2.11 MPa (95% CI 1.97–2.25) at 0.5 MHz, 2.54 MPa (95% CI 2.47–2.62) at 1 MHz and 3.29 MPa (95% CI 3.08–3.50) at 1.5 MHz. However, in the presence of nanodroplets, a substantially lower pressure was required to achieve the same extravasation depth (0.40 MPa (95% CI 0.30–0.49) at 0.5 MHz, 1.21 MPa (95% CI 1.12–1.30) at 1 MHz, and 1.62 MPa (95% CI 1.47–1.76) at 1.5 MHz) indicating that PFB NDs can enhance the extravasation of nanospheres. The driving frequency significantly impacts the extravasation depth. The same experiments were conducted using PFB NDs loaded with Nile red. The extravasation depth of Nile red increased with escalating driving pressures at each ultrasound frequency, as depicted in Figure 9d. The pressure required to achieve an extravasation depth of 0.3 mm was 0.39 MPa (95% CI 0.30–0.49) at 0.5 MHz, 1.14 MPa (95% CI 1.07–1.20) at 1 MHz and 1.46 MPa (95% CI 1.32–1.60) at 1.5 MHz. These findings paralleled the results observed when nanospheres were mixed with nanodroplets, with a correlation coefficient between extravasation depths of 0.994 (95% CI 0.984 –0.998) across all frequencies. It is noteworthy that the maximum extravasation depth was constrained to 5.5 mm by the phantom thickness. Thus, at 2.5 MPa and 0.5 MHz, the extravasation depth represented the maximum penetration achievable. Upon further increasing the pressure to 3 MPa, the extravasation depth at 1 MHz reached the maximum depth, and at 1.5 MHz, it was 2.7 ± 0.5 mm. This is in agreement with the authors' previous findings that both vaporization and IC thresholds increase with increasing frequency. It suggests however that using an IC threshold defined as PIC>80% overestimates the pressure required to achieve substantial extravasation. In contrast to the findings of previous studies involving higher molecular weight PFCs [9], the results of this study suggest that PFB NDs can act as effective cavitation agents enabling extravasation of both types of model drug in a tissue phantom at comparable acoustic pressures to those required by gas microbubbles and solid nuclei.

Cytotoxicity and cellular uptake of PFB NDs

The cytotoxicity of PFB NDs was assessed using an MTS assay according to the manufacturer's protocol. Figure 10a displays the viability of A549 cells measured after incubation with unloaded PFB NDs at various concentrations. Cytotoxicity, (BMD) was found to be low, requiring, with a BMD of 9.4 $x10^{10}$ NDs/ml to produce a 15% decrease in cell viability (95% CI 5.2 x 10^{10}–1.4 x 10^{11}). No apparent sign of damage or inflammation was observed by optical microscopy. Additionally, the cellular uptake of PFB NDs was investigated, revealing that DiO-labelled PFB NDs (depicted in green in Figure 10(b)) were readily taken up by A549 cells. The mechanism of uptake in A549 cells is likely mediated through endocytosis, as suggested by previous research findings [19–25]. It should be noted that the uptake of nanoparticles by A549 cells was found to be a time-, temperature-, energy- and concentration-dependent saturable event mediated by endocytic pathways [20,21,24]. This characteristic could be usefully exploited in drug delivery applications.

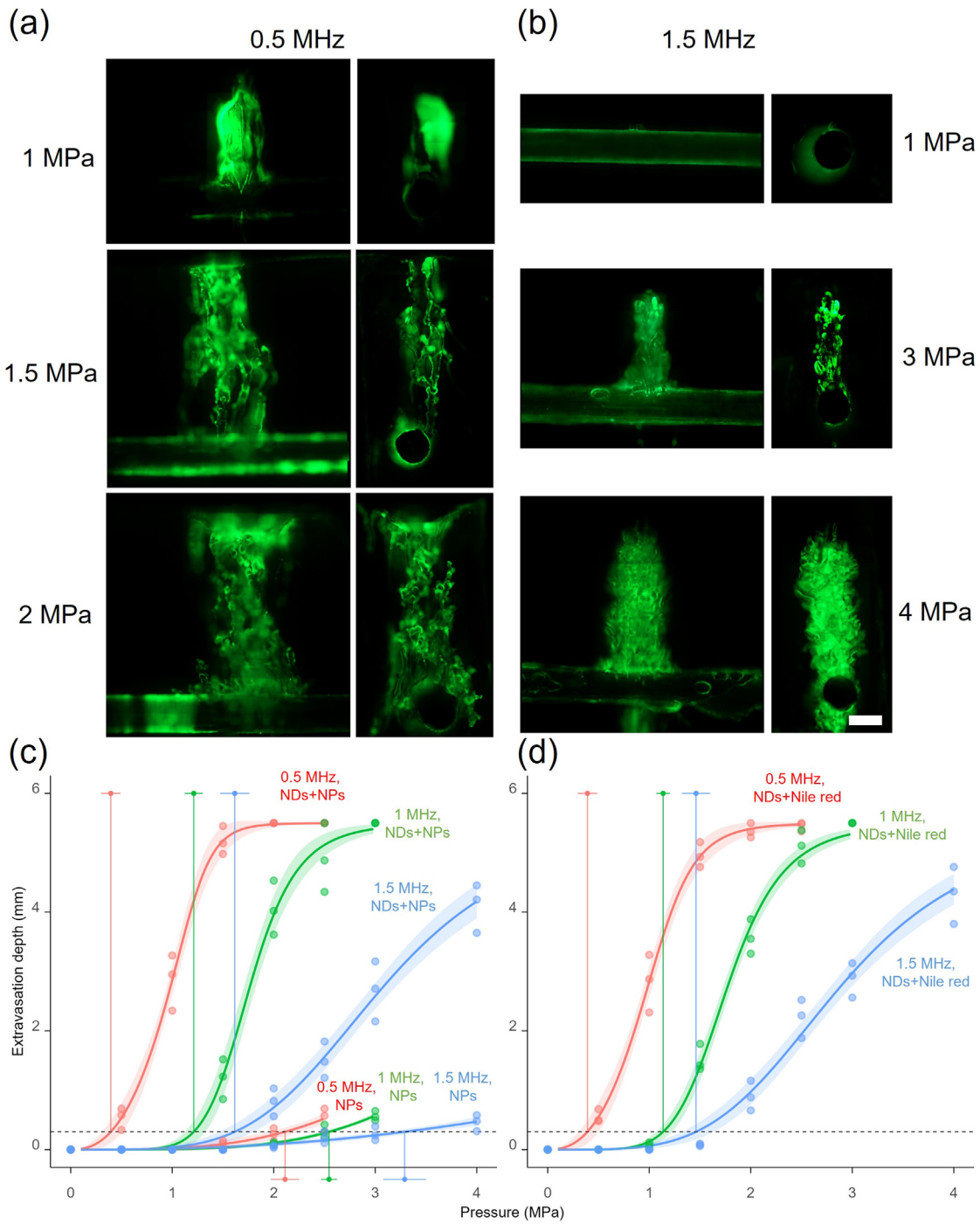

Figure 9. Representative microscopy images of nanosphere extravasation in the agarose phantom model under different ultrasound pressures at 0.5 MHz (a) and 1.5 MHz (b) at the same duty cycle (5%), showing green fluorescence images of the top (left) and side (right) view of channel. The scale bar is 1 mm. Effect of ultrasound frequency and pressure on cavitation-mediated extravasation using nanospheres (c) and Nile red (d) as model drug. The solid lines are fitted concentrations, and the shaded areas are simultaneous 95% confidence bands. Pressure thresholds are shown above (for NDs + NPs and NDs + Nile red) or below (for NPs) the plots as points with horizontal error bars, corresponding to their 95% confidence intervals.

Limitations of the study

As mentioned above, ND stability was only measured in water and PBS, and further investigations of ND stability in blood is required to assess the potential for spontaneous vaporization and any corresponding risk. For convenience in measuring the stability and drug release of nanodroplets, highly concentrated formulations were utilized. However, diluting these nanodroplets to concentrations similar to those used in *in vitro* cellular experiments or *in vivo* studies may reveal more rapid destabilization kinetics. Therefore, the concentration-dependent stability profiles of nanodroplets necessitate further investigation. Such research is essential for elucidating the NDs behaviour under conditions that closely replicate actual experimental or clinical settings.

The type of flow phantom used in this study has been shown to be predictive of the mechanical behaviour of some tissues [26], but experiments in actual tissue, both healthy and diseased, will be needed to accurately quantify the degree of extravasation that can be expected for different ultrasound exposure conditions. Similarly, the channel

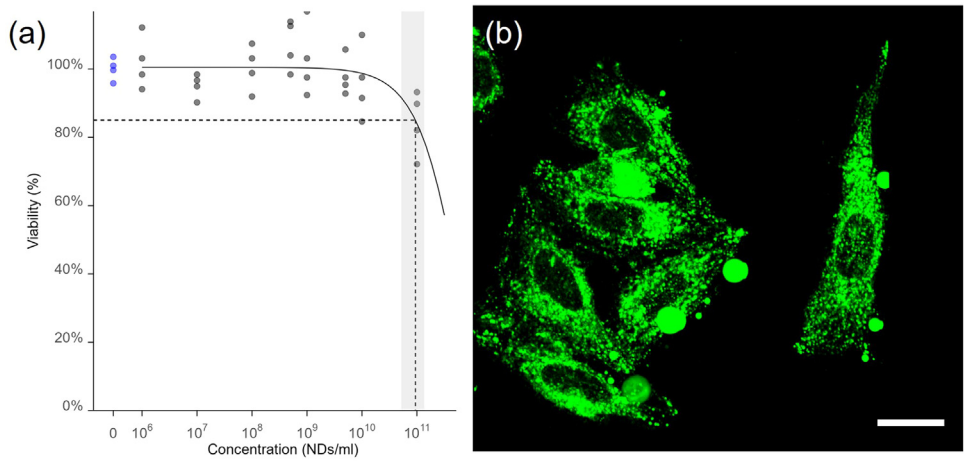

Figure 10. (a) The viability of cells incubated with different concentrations of PFB NDs ranging from 10^6 to 10^{11} particles/mL for 24 h. (The vertical dashed line indicates the BMD, while the shaded area indicates the corresponding 95% confidence interval). (b) Confocal image of DiO-loaded PFB NDs uptake by A549 cells. The scale bar is 20 μm.

diameter used in this study was large compared with that of microvessels in e.g. a tumour. It is well known that confinement influences bubble dynamics [27] and vessel size would thus also be expected to affect the relationship between driving ultrasound pressure and extravasation. The characteristics of different drug molecules and/or other therapeutic ingredients might also affect their transport in tissue; e.g. liposomes might behave differently from solid nanoparticles.

Conclusions

This study investigated the potential utility of perfluorobutane (PFB) nanodroplets (NDs) as cavitation agents to promote drug extravasation. In a tissue mimicking phantom, extravasation of two model drugs (Nile Red simulating a small molecule drug and 200 nm polymer beads simulating a larger therapeutic agent) was observed over a range of ultrasound exposure conditions corresponding to the frequencies and pressures typically used in ultrasound mediated drug delivery (0.5 −1.5 MHz and 0.5−3.5 MPa, respectively). Contrary to the findings of previous studies with higher molecular weight PFCs, PFB NDs were not found to require substantially higher acoustic pressures than those used with other types of cavitation nuclei (such as gas microbubbles) to achieve comparable extravasation. At a driving frequency of 0.5 MHz, the peak negative pressure required to achieve 80% probability of inertial cavitation (PIC) was 1.25 ± 0.13 MPa at 37°C. This threshold rose with increasing the driving frequency and was correlated with the number of vaporization events observed using ultra high-speed imaging, consistent with previous work [10]. Moreover, as an indicator of extravasation, PIC was found to be a conservative metric. Notably, extravasation depths of several mm were observed for both model drugs at peak negative pressures below the 80% PIC threshold. PFB NDs were found to be stable in water at both 4°C and 37°C in the absence of ultrasound exposure. They had no effect on the viability of A549 cancer cells up to concentrations of 10^{10} ND/ml and were also readily taken up intact by this cell line. Further work is needed to assess the stability of PFB NDs in whole blood and to quantify extravasation in real vessels of different sizes in tissues having different mechanical properties.

Conflict of interest

The authors declare no conflicts of interest.

Data availability statement

All data not already provided in the manuscript or supplementary material may be obtained from the corresponding author upon request.

Acknowledgments

The authors are grateful to the Engineering and Physical Sciences Research Council (EPSRC) for supporting this research through Grant EP/R013624/1. The authors also thank Mr. James Fisk of the IBME workshop for construction of the apparatus used in this study; Dr. Errin Johnson and Dr. Adam Costin of the Dunn School Bioimaging Facility for their kind assistance with the Cryo-EM; Dr. Veerle Brans of BUBBL lab for supporting with the A549 cell line, Dr. Michael Gray of BUBBL lab for supporting with the SAT2 setup.

Supplementary materials

Supplementary material associated with this article can be found, in the online version, at doi:10.1016/j.ultrasmedbio.2024.06.016.

References

[1] Rapoport N. Phase-shift, stimuli-responsive perfluorocarbon nanodroplets for drug delivery to cancer. Wiley Interdiscip Rev Nanomed Nanobiotechnol 2012;4:492–510. doi: 10.1002/WNAN.1176.
[2] Kripfgans OD, Fowlkes JB, Miller DL, Eldevik OP, Carson PL. Acoustic droplet vaporization for therapeutic and diagnostic applications. Ultrasound Med Biol 2000;26:1177–89.
[3] Ho YJ, Chang YC, Yeh CK. Improving nanoparticle penetration in tumors by vascular disruption with acoustic droplet vaporization. Theranostics 2016;6:392–403. doi: 10.7150/thno.13727.
[4] Feng Y, Qin D, Zhang J, Zhang L, Bouakaz A, Wan MX. Occlusion and rupture of ex vivo capillary bifurcation due to acoustic droplet vaporization. Appl Phys Lett 2018;112. doi: 10.1063/1.5025594.
[5] Helfield BL, Yoo K, Liu J, Williams R, Sheeran PS, Goertz DE, et al. Investigating the accumulation of submicron phase-change droplets in tumors. Ultrasound Med Biol 2020;46:2861–70. doi: 10.1016/J.ULTRASMEDBIO.2020.06.021.
[6] Durham PG, Dayton PA. Applications of sub-micron low-boiling point phase change contrast agents for ultrasound imaging and therapy. Curr Opin Colloid Interface Sci 2021;56:101498. doi: 10.1016/J.COCIS.2021.101498.
[7] Sheeran P, Luois S, Dayton PA, Matsunaga T. Formulation and acoustic studies of new phase-shift agent for diagnostic and therapeutic ultrasound. Langmuir 2011;27:10412–20.
[8] Gouveia FV, Lea-Banks H, Aubert I, Lipsman N, Hynynen K, Hamani C. Anesthetic-loaded nanodroplets with focused ultrasound reduces agitation in Alzheimer's mice. Ann Clin Transl Neurol 2023;10:507–19. doi: 10.1002/ACN3.51737.
[9] Mannaris C, Bau L, Grundy M, Gray M, Lea-Banks H, Seth A, et al. Microbubbles, nanodroplets and gas-stabilizing solid particles for ultrasound-mediated extravasation of unencapsulated drugs: an exposure parameter optimization study. Ultrasound Med Biol 2019;45:954–67. doi: 10.1016/j.ultrasmedbio.2018.10.033.
[10] Wu Q, Mannaris C, May JP, Bau L, Polydorou A, Ferri S, et al. Investigation of the acoustic vaporization threshold of lipid-coated perfluorobutane nanodroplets using both high-speed optical imaging and acoustic methods. Ultrasound Med Biol 2021;47:1826–43. doi: 10.1016/J.ULTRASMEDBIO.2021.02.019.
[11] Mannaris C, Teo BM, Seth A, Bau L, Coussios C, Stride E. Gas-stabilizing gold nanocones for acoustically mediated drug delivery. Adv Healthc Mater 2018;7:1800184. doi: 10.1002/ADHM.201800184.

[12] Gray M, Vasilyeva AV, Brans V, Stride E. Studying cavitation enhanced therapy. JoVE (J Visualized Exp) 2021;2021:e61989. doi: 10.3791/61989.
[13] Hobbs SK, Monsky WL, Yuan F, Roberts WG, Griffith L, Torchilin VP, et al. Regulation of transport pathways in tumor vessels: role of tumor type and microenvironment. Proc Natl Acad Sci 1998;95:4607–12. doi: 10.1073/PNAS.95.8.4607.
[14] Hoshyar N, Gray S, Han H, Bao G. The effect of nanoparticle size on in vivo pharmacokinetics and cellular interaction. Nanomedicine 2016;11:673–92. doi: 10.2217/NNM.16.5.
[15] McComiskey KPM, Tajber L. Comparison of particle size methodology and assessment of nanoparticle tracking analysis (NTA) as a tool for live monitoring of crystallisation pathways. Eur J Pharmaceut Biopharmaceut 2018;130:314–26. doi: 10.1016/J.EJPB.2018.07.012.
[16] Mountford PA, Sirsi SR, Borden MA. Condensation phase diagrams for lipid-coated perfluorobutane microbubbles. Langmuir 2014;30:6209–18. doi: 10.1021/LA501004U/SUPPL_FILE/LA501004U_SI_001.PDF.
[17] Schroeder A, Avnir Y, Weisman S, Najajreh Y, Gabizon A, Talmon Y, et al. Controlling liposomal drug release with low frequency ultrasound: mechanism and feasibility. Langmuir 2007;23:4019–25. doi: 10.1021/LA0631668/ASSET/IMAGES/LARGE/LA0631668F00010.JPEG.
[18] Yu Lee J, Carugo D, Crake C, Owen J, de Saint Victor M, Seth A, et al. Nanoparticle-loaded protein−polymer nanodroplets for improved stability and conversion efficiency in ultrasound imaging and drug delivery. Adv Mater 2015;27:5484–92. doi: 10.1002/ADMA.201502022.
[19] Kuhn DA, Vanhecke D, Michen B, Blank F, Gehr P, Petri-Fink A, et al. Different endocytotic uptake mechanisms for nanoparticles in epithelial cells and macrophages. Beilstein J Nanotechnol 2014;174(5):1625–36. doi: 10.3762/BJNANO.5.174.
[20] Kim JS, Yoon TJ, Yu KN, Mi SN, Woo M, Kim BG, et al. Cellular uptake of magnetic nanoparticle is mediated through energy-dependent endocytosis in A549 cells. J Vet Sci 2006;7:321. doi: 10.4142/JVS.2006.7.4.321.
[21] Mo Y, Lim LY. Mechanistic study of the uptake of wheat germ agglutinin-conjugated PLGA nanoparticles by A549 cells. J Pharm Sci 2004;93:20–8. doi: 10.1002/JPS.10507.
[22] Tahara K, Sakai T, Yamamoto H, Takeuchi H, Hirashima N, Kawashima Y. Improved cellular uptake of chitosan-modified PLGA nanospheres by A549 cells. Int J Pharm 2009;382:198–204. doi: 10.1016/J.IJPHARM.2009.07.023.
[23] Martins S, Costa-Lima S, Carneiro T, Cordeiro-Da-Silva A, Souto EB, Ferreira DC. Solid lipid nanoparticles as intracellular drug transporters: An investigation of the uptake mechanism and pathway. Int J Pharm 2012;430:216–27. doi: 10.1016/J.IJPHARM.2012.03.032.
[24] Tahara K, Yamamoto H, Kawashima Y. Cellular uptake mechanisms and intracellular distributions of polysorbate 80-modified poly (d,l-lactide-co-glycolide) nanospheres for gene delivery. Eur J Pharmaceut Biopharmaceut 2010;75:218–24. doi: 10.1016/J.EJPB.2010.03.013.
[25] Zhang YL, Zhang ZH, Jiang TY, Ayman-Waddad Jing-Li, Lv HX, et al. Cell uptake of paclitaxel solid lipid nanoparticles modified by cell-penetrating peptides in A549 cells. Pharmazie 2013;68:47–53. doi: 10.1691/PH.2013.2071.
[26] Manickam K, Machireddy RR, Seshadri S. Characterization of biomechanical properties of agar based tissue mimicking phantoms for ultrasound stiffness imaging techniques. J Mech Behav Biomed Mater 2014;35:132–43. doi: 10.1016/J.JMBBM.2014.03.017.
[27] Zhao X, Wright A, Goertz DE. An optical and acoustic investigation of microbubble cavitation in small channels under therapeutic ultrasound conditions. Ultrason Sonochem 2023;93:106291. doi: 10.1016/J.ULTSONCH.2023.106291.
[28] Zhao Y, Shi D, Guo L, Shang M, Sun X, Meng D, et al. Ultrasound targeted microbubble destruction-triggered nitric oxide release via nanoscale ultrasound contrast agent for sensitizing chemoimmunotherapy. J Nanobiotechnol 2023;21:1–17. doi: 10.1186/S12951-023-01776-8/FIGURES/8.
[29] Xiao H, Li X, Li B, Zhong Y, Qin J, Wang Y, et al. Sono-promoted drug penetration and extracellular matrix modulation potentiate sonodynamic therapy of pancreatic ductal adenocarcinoma. Acta Biomater 2023;161:265–74. doi: 10.1016/J.ACTBIO.2023.02.038.
[30] Samani RK, Maghsoudinia F, Mehradnia F, Hejazi SH, Saeb M, Sobhani T, et al. Ultrasound-guided chemoradiotherapy of breast cancer using smart methotrexate-loaded perfluorohexane nanodroplets. Nanomedicine 2023;48:102643. doi: 10.1016/J.NANO.2022.102643.
[31] Yamaguchi S, Kisaka M, Higashi K, Ishijima A, Azuma T, Nakagawa K, et al. Cytosolic protein delivery using ultrasound-guided vaporization of perfluorocarbon nanodroplets. Biotechnol J 2023;18:2300018. doi: 10.1002/BIOT.202300018.
[32] Hou J, Zhou J, Chang M, Bao G, Xu J, Ye M, et al. LIFU-responsive nanomedicine enables acoustic droplet vaporization-induced apoptosis of macrophages for stabilizing vulnerable atherosclerotic plaques. Bioact Mater 2022;16:120–33. doi: 10.1016/J.BIOACTMAT.2022.02.022.
[33] Zamani R, Bizari D, Heiat M. Synthesis and characterization of phase shift dextran stabilized nanodroplets for ultrasound-induced cancer therapy: a novel nanobiotechnology approach. J Biotechnol 2022;350:17–23. doi: 10.1016/J.JBIOTEC.2022.04.003.
[34] Shar A, Aboutalebianaraki N, Misiti K, Sip YYL, Zhai L, Razavi M. A novel ultrasound-mediated nanodroplet-based gene delivery system for osteoporosis treatment. Nanomedicine 2022;41. doi: 10.1016/J.NANO.2022.102530.
[35] Wang X, Shang M, Sun X, Guo L, Xiao S, Shi D, et al. Dual-responsive nanodroplets combined with ultrasound-targeted microbubble destruction suppress tumor growth and metastasis via autophagy blockade. J Control Release 2022;343:66–77. doi: 10.1016/J.JCONREL.2022.01.009.
[36] Gao Y, Ma Q, Cao J, Shi Y, Wang J, Ma H, et al. Bifunctional alginate/chitosan stabilized perfluorohexane nanodroplets as smart vehicles for ultrasound and pH responsive delivery of anticancer agents. Int J Biol Macromol 2021;191:1068–78. doi: 10.1016/J.IJBIOMAC.2021.09.166.
[37] Xie Z, Wang J, Luo Y, Qiao B, Jiang W, Zhu L, et al. Tumor-penetrating nanoplatform with ultrasound "unlocking" for cascade synergistic therapy and visual feedback under hypoxia. J Nanobiotechnology 2023;21:1–20. doi: 10.1186/S12951-023-01765-X/FIGURES/9.
[38] Spatarelu CP, Jandhyala S, Luke GP. Dual-drug loaded ultrasound-responsive nanodroplets for on-demand combination chemotherapy. Ultrasonics 2023;133:107056. doi: 10.1016/J.ULTRAS.2023.107056.
[39] Huang S, Guo W, An J, Zhang J, Dong F, Wang D, et al. Enhanced acoustic droplet vaporization through the active magnetic accumulation of drug-loaded magnetic particle-encapsulated nanodroplets (MPE-NDs) in cancer therapy. Nano Lett 2022;22:8143–51. doi: 10.1021/ACS.NANOLETT.2C02580/SUPPL_FILE/NL2C02580_SI_002.AVI.
[40] Xi L, Han Y, Liu C, Liu Y, Wang Z, Wang R, et al. Sonodynamic therapy by phase-transition nanodroplets for reducing epidermal hyperplasia in psoriasis. Journal of Controlled Release 2022;350:435–47. doi: 10.1016/J.JCONREL.2022.08.038.
[41] Yang D, Chen Q, Zhang M, Feng G, Sun D, Lin L, et al. Drug-loaded acoustic nanodroplet for dual-imaging guided highly efficient chemotherapy against nasopharyngeal carcinoma. Int J Nanomedicine 2022;17:4879–94. doi: 10.2147/IJN.S377514.
[42] Yang C, Zhang Y, Luo Y, Qiao B, Wang X, Zhang L, et al. Dual ultrasound-activatable nanodroplets for highly-penetrative and efficient ovarian cancer theranostics. J Mater Chem B 2020;8:380–90. doi: 10.1039/C9TB02198A.
[43] Dong W, Wu P, Zhou D, Huang J, Qin M, Yang X, et al. Ultrasound-mediated gene therapy of hepatocellular carcinoma using Pre-microRNA plasmid-loaded nanodroplets. Ultrasound Med Biol 2020;46:90–107. doi: 10.1016/J.ULTRASMEDBIO.2019.09.016.
[44] Zhang L, Yi H, Song J, Huang J, Yang K, Tan B, et al. Mitochondria-targeted and ultrasound-activated nanodroplets for enhanced deep-penetration sonodynamic cancer therapy. ACS Appl Mater Interfaces 2019;11:9355–66. doi: 10.1021/acsami.8b21968.
[45] Ho YJ, Chiang YJ, Kang ST, Fan CH, Yeh CK. Camptothecin-loaded fusogenic nanodroplets as ultrasound theranostic agent in stem cell-mediated drug-delivery system. J Control Release 2018;278:100–9. doi: 10.1016/J.JCONREL.2018.04.001.
[46] Lee JY, Crake C, Teo B, Carugo D, de Saint, Victor M, Seth A, et al. Ultrasound-enhanced siRNA delivery using magnetic nanoparticle-loaded chitosan-deoxycholic acid nanodroplets. Adv Healthc Mater 2017;6:1601246. doi: 10.1002/ADHM.201601246.
[47] Wang CH, Kang ST, Lee YH, Luo YL, Huang YF, Yeh CK. Aptamer-conjugated and drug-loaded acoustic droplets for ultrasound theranosis. Biomaterials 2012;33:1939–47. doi: 10.1016/J.BIOMATERIALS.2011.11.036.
[48] Lea-Banks H, Hynynen K. Sub-millimetre precision of drug delivery in the brain from ultrasound-triggered nanodroplets. J Control Release 2021;338:731–41. doi: 10.1016/J.JCONREL.2021.09.014.
[49] Lea-Banks H, O'Reilly MA, Hamani C, Hynynen K. Localized anesthesia of a specific brain region using ultrasound-responsive barbiturate nanodroplets. Theranostics 2020;10:2849. doi: 10.7150/THNO.41566.
[50] Wu SY, Fix SM, Arena CB, Chen CC, Zheng W, Olumolade OO, et al. Focused ultrasound-facilitated brain drug delivery using optimized nanodroplets: vaporization efficiency dictates large molecular delivery. Phys Med Biol 2018;63:035002. doi: 10.1088/1361-6560/AAA30D.
[51] Honari A, Merillat DA, Bellary A, Ghaderi M, Sirsi SR. Improving release of liposome-encapsulated drugs with focused ultrasound and vaporizable droplet-liposome nanoclusters. Pharmaceutics 2021;13:609. doi: 10.3390/PHARMACEUTICS13050609/S1.
[52] Fix SM, Koppolu BP, Novell A, Hopkins J, Kierski TM, Zaharoff DA, et al. Ultrasound-stimulated phase-change contrast agents for transepithelial delivery of macromolecules, toward gastrointestinal drug delivery. Ultrasound Med Biol 2019;45:1762–76. doi: 10.1016/J.ULTRASMEDBIO.2019.02.004.
[53] Fix SM, Novell A, Escoffre JM, Tsuruta JK, Dayton PA, Bouakaz A. In-vitro delivery of BLM into resistant cancer cell line using sonoporation with low-boiling point phase change ultrasound contrast agents. IEEE Int Ultrasonics Symposium, IUS 2017:1. doi: 10.1109/ULTSYM.2017.8091622.
[54] Choi M, Jazani AM, Oh JK, Noh SM. Perfluorocarbon nanodroplets for dual delivery with ultrasound/GSH-responsive release of model drug and passive release of nitric oxide. Polymers (Basel) 2022;14:2240. doi: 10.3390/POLYM14112240.